Phase 1 Evaluation of ^{11}C-CS1P1 to Assess Safety and Dosimetry in Human Participants

Matthew R. Brier[1], Mahdjoub Hamdi[2], Jayashree Rajamanikam[2], Haiyang Zhao[2], Syahir Mansor[2], Lynne A. Jones[2], Farzaneh Rahmani[2], Saurabh Jindal[2], Deborah Koudelis[2], Joel S. Perlmutter[1–4], Dean F. Wong[1–3,5], Michael Nickels[2], Joseph E. Ippolito[2], Robert J. Gropler[2], Thomas H. Schindler[2], Richard Laforest[2], Zhude Tu[2], and Tammie L.S. Benzinger[2]

[1]Department of Neurology, Washington University, St. Louis, Missouri; [2]Mallinckrodt Institute of Radiology, Washington University, St. Louis, Missouri; [3]Department of Neuroscience, Washington University, St. Louis, Missouri; [4]Department of Physical and Occupational Therapy, Washington University, St. Louis, Missouri; and [5]Department of Psychiatry, Washington University, St. Louis, Missouri

This study evaluated the safety, dosimetry, and characteristics of 3-((2-fluoro-4-(5-(2′-methyl-2-(trifluoromethyl)-[1,1′-biphenyl]-4-yl)-1,2,4-oxadiazol-3-yl)benzyl)(methyl-^{11}C)amino)propanoic acid (^{11}C-CS1P1), a radiotracer targeting sphingosine-1-phosphate receptor (S1PR) 1 (S1PR1). S1PR1 is of clinical interest because of its role in multiple sclerosis (and other conditions), with an expanding class of S1PR modulators approved for relapsing multiple sclerosis. ^{11}C-CS1P1 binds S1PR1 with high specificity and has shown promise in animal models of inflammatory diseases. **Methods:** ^{11}C-CS1P1 was injected into 5 male and 6 female healthy participants. Ten participants were imaged with PET using a multipass whole-body continuous-bed-motion acquisition, and one had dedicated head and neck PET and MRI. Participants were continuously monitored for safety events. Organ time–activity curve data were collected, integrated, and normalized to the injected activity. Organ radiation doses and effective dose were computed using the adult male and female models in OLINDA, version 2.2. SUV images were evaluated for qualitative biodistribution. **Results:** No adverse events were observed after the dose, including no bradycardia. The liver was the critical organ from dosimetry analysis (mean ± SD: female, 23.12 ± 5.19 μSv/MBq; male, 21.06 ± 1.63 μSv/MBq). The whole-body effective dose (as defined by International Commission on Radiological Protection publication 103) was 4.18 ± 0.30 μSv/MBq in women and 3.54 ± 0.14 μSv/MBq in men. Using a maximum delivered dose of 740 MBq (20 mCi), the effective dose for women would be 3.1 mSv (0.31 rem), with a liver dose of 17.1 mSv (1.7 rem); the effective dose for men would be 2.6 mSv (0.26 rem), with a liver dose of 15.6 mSv (1.56 rem). Brain uptake was seen predominantly in gray matter and correlated with regional S1PR1 RNA expression (r = 0.84). **Conclusion:** These results support the safety of ^{11}C-CS1P1 for evaluation of inflammation in human clinical populations. Dosimetry permits repeated measures in the same participants. Brain uptake correlates well with known target topography.

Key Words: sphingosine-1-phosphate; spingosine-1-phosphate receptors; PET; cerebral inflammation; radiation dosimetry

J Nucl Med 2022; 63:1775–1782
DOI: 10.2967/jnumed.121.263189

Received Oct. 3, 2021; revision accepted Mar. 2, 2022.
For correspondence or reprints, contact Tammie L.S. Benzinger (benzingert@wustl.edu) or Zhude Tu (zhudetu@wustl.edu).
Published online Mar. 24, 2022.

Sphingosine-1-phosphate (S1P) is a membrane-derived lysophospholipid that plays a regulatory role in inflammatory diseases, including multiple sclerosis (*1*) and inflammatory bowel disease (*2*). S1P signals via 5 G-protein–coupled receptors (S1PR1–5) (*3*). S1PR1 is expressed on a variety of tissues, including endothelial cells, vascular smooth muscle cells, astrocytes, and lymphocytes (*4,5*). Treatment with any of 4 Food and Drug Administration–approved S1PR1 modulators sequesters lymphocytes within lymph nodes (*6*), thereby reducing relapses in multiple sclerosis patients (*7*). In addition to lymphoid effects, S1PR1 modulation also inhibits microglial activation (*8*), improves remyelination after injury (*9*), and promotes oligodendrocyte survival (*5*), presumably mediated by astrocyte signaling (*10*). Thus, in vivo imaging of S1PR1 could contribute to the understanding of multiple sclerosis and other inflammatory disorders, including response to treatment.

S1PR1 signaling plays an important role beyond prototypic inflammatory disorders. For example, high S1PR1 expression relates to higher mortality in estrogen receptor–positive breast cancer (*11*). Similarly, S1PR1 partially regulates neovascularization of tumors (*12*) and modulates expression of hypoxia-inducible factor 2 α, which can drive aggressive malignancy (*13*).

A recently developed radiotracer, 3-((2-fluoro-4-(5-(2′-methyl-2-(trifluoromethyl)-[1,1′-biphenyl]-4-yl)-1,2,4-oxadiazol-3-yl)benzyl)(methyl-^{11}C)amino)propanoic acid (^{11}C-CS1P1), shows increased binding in an experimental autoimmune encephalomyelitis rodent model (*4*), after carotid artery injury (*14*), and within atherosclerotic plaques (*15*). Safety and dosimetry studies in a rodent model demonstrated good safety and low radiation dose exposure compatible with first-in-humans testing (*16*). This paper reports on the safety, radiation dosimetry, and initial imaging results of ^{11}C-CS1P1 in 11 healthy human volunteers.

MATERIALS AND METHODS

Study Design and Participants

This study was preregistered on ClinicalTrials.gov (NCT04517552), approved by the Washington University Institutional Review Board and Radioactive Drug Research Committee, and performed under Food and Drug Administration Investigational New Drug Application 146548. All participants provided written informed consent. The dosimetry cohort consisted of 10 healthy participants (5 male and 5 female) who underwent whole-body PET/CT imaging. Additionally, 1 female participant underwent dedicated brain imaging. The inclusion

TABLE 1
Participant Demographics and Injected Dose

Demographic	Participant no.									
	1	2	3	4	5	6	7	8	9	10
Sex	M	F	F	M	M	M	M	F	F	F
Age (y)	28	23	40	61	59	34	37	27	27	39
Height (cm)	185.4	177.8	165.1	167.6	185.4	175.3	172.7	165.1	162.6	175.3
Weight (kg)	88.9	105.7	69.4	67.1	104.8	106.1	74.8	117.9	50.3	117.5
Injected dose										
MBq	266.4	99.9	170.2	247.9	240.5	296.0	225.7	210.9	362.6	144.3
mCi	7.2	2.7	4.6	6.7	6.5	8.0	6.1	5.7	9.8	3.9
Injected mass (μg)	4.70	4.56	3.29	2.88	2.69	3.40	2.94	3.27	2.78	0.98

criteria were any sex or race, age greater than 18 y, capability of providing written informed consent to undergo research procedures, and general health, without major neurologic disease (e.g., epilepsy). The exclusion criteria included hypersensitivity to ^{11}C-CS1P1 or any of its excipients, contraindications to PET or CT, severe claustrophobia, pregnancy or breastfeeding, conditions that could increase the risk of study participation (e.g., renal or liver failure), current radiation therapy, or a history of unstable arrhythmias or indications of cardiovascular disease. The cardiac disease–related exclusion derives from the association between S1P-modulating drugs and clinically significant bradycardia (*7*), despite the small injected mass of radiopharmaceutical.

Radiopharmaceutical Synthesis

The ^{11}C-CS1P1 was radiosynthesized by alkylating the precursor with ^{11}C-methyl triflate in acetonitrile at 60°C for 5 min, followed by removing the t-butyl group using trifluoroacetic acid, and purifying using reverse-phase high-performance liquid chromatography (*17*).

Dosimetry Cohort PET/CT Image Acquisition

Ten dosimetry participants were imaged using a Biograph Vision PET/CT scanner (Siemens Healthineers). Low-dose CT was performed from the vertex to midthigh before PET imaging for anatomic alignment and attenuation correction (120 kVp, 50 mAs). After injection of ^{11}C-CS1P1 and a saline flush, dynamic images were obtained over the heart for 5 min, followed by whole-body dynamic acquisitions in continuous bed motion. Acquisition involving only the heart for the first 5 min was done for 2 reasons: first, to allow for capturing the high amount of radioactivity in the blood volume in the heart immediately after injection and, second, to facilitate the required electrocardiogram. Whole-body sweep epochs were 120 s (×11), 300 s (×6), and 600 s (×6) over approximately 2 h using a continuous-bed-motion acquisition. PET images were reconstructed using a 3-dimensional (3D) ordered-subset expectation maximization algorithm with time-of-flight and point-spread-function resolution modeling (4 iterations and 5 subsets) with no postreconstruction filtering. Images were inspected for evidence of motion, and alignment was manually corrected, if needed.

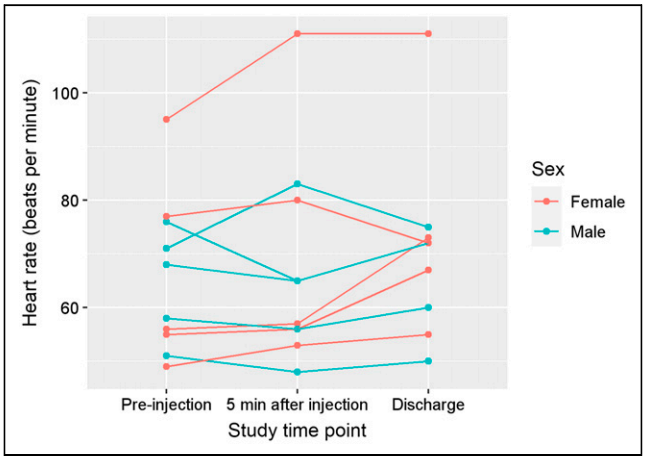

FIGURE 1. Heart rate response to ^{11}C-CS1P1 injection: stable heart rate before injection, 5 min after injection, and at discharge, as captured on 12-lead electrocardiogram ($P > 0.1$).

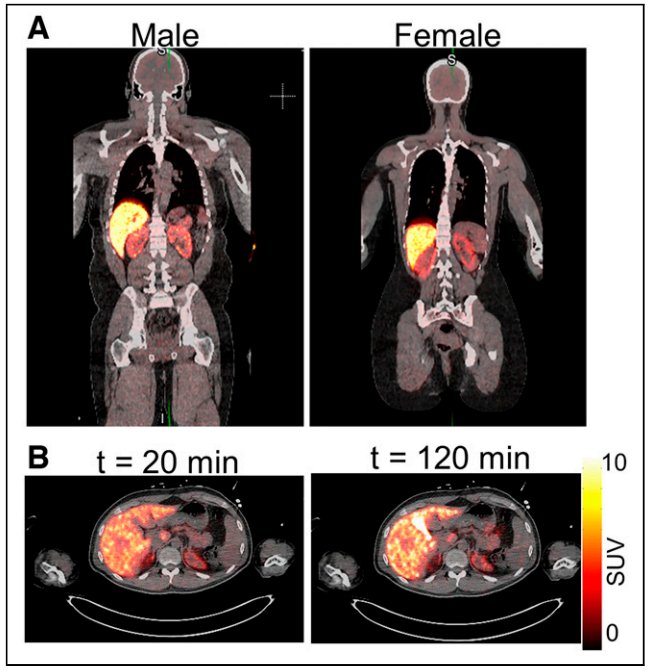

FIGURE 2. Qualitative biodistribution of ^{11}C-CS1P1. (A) Summed activity PET/CT images for representative male and female participants. (B) Decay-corrected activity is high in liver early in scanning session but is clearly concentrated in gallbladder later in scans, compatible with hepatobiliary excretion.

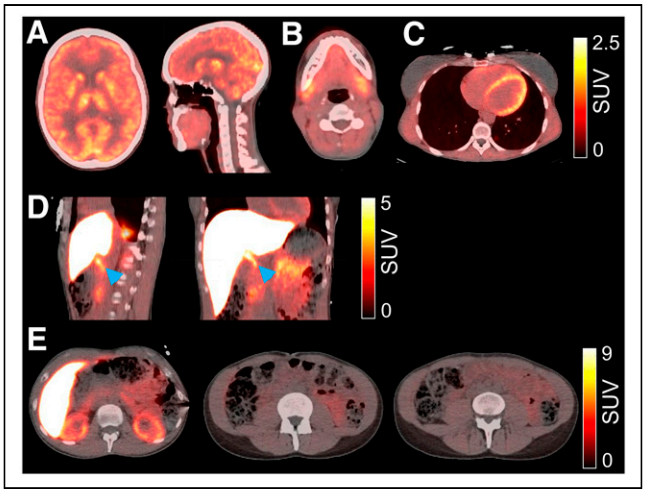

FIGURE 3. Qualitative biodistribution in typical participant. Summed activity on ^{11}C-CS1P1 PET/CT images is expressed as SUV. (A–D) Uptake in brain is highest in gray matter and relatively low in white matter. Increased update is seen in salivary glands (B), left ventricle (C), and liver (D). Common bile duct is appreciated (arrowhead). (E) Parenchymal uptake within kidneys is seen but without activity in collecting system and with scant amounts of small-bowel uptake.

Pharmaceutical Safety Evaluation

Safety of the injected dose was assessed in several ways. First, serial electrocardiograms (at enrollment, before injection, 5 min after injection, and then hourly until discharge) were obtained and the patient was monitored on telemetry to assess for bradycardia (heart rate $<$ 40 bpm) or other significant arrhythmias (atrial fibrillation or flutter, reentrant tachycardia, second- or third-degree heart block, or ventricular arrhythmia). Similarly, patients were monitored for hypotension (systolic blood pressure $<$ 100 mmHg, diastolic blood pressure $<$ 70 mmHg). Laboratory evaluation after injection consisted of a complete blood count, comprehensive metabolic panel, and urinalysis and was compared with baseline measures. Finally, all participants were contacted 2–3 d after the study to assess for any delayed adverse events.

Qualitative Biodistribution

Whole-body CT scans underwent a standard-of-care review by board-certified radiologists. After image acquisition, merged CT and ^{11}C-CS1P1 PET images were reviewed again to identify potential findings of interest regarding ^{11}C-CS1P1.

Radiation Dosimetry

Volumes of interest were manually traced over source organs with measurable activity: brain, lungs, cardiac muscle, lung, liver, spleen, kidney, small intestine, urinary bladder, and muscle. Organs with well-defined boundaries were contoured in their entirety (e.g., liver and kidneys). Organs with complex boundaries (e.g., small bowel) or impacted by respiratory motion (e.g., heart and lungs) were sampled and activity scaled to the estimated mass of the organ. Time–activity curves were obtained for each source organ by expressing the total activity (non–decay-corrected) in the volume of interest as a percentage of total injected activity. Numerically integrated time–activity values were entered into OLINDA, version 2.2 (Hermes), to calculate organ doses and effective dose (as defined by International Commission on Radiological Protection publication 103) (*18*) using the International Commission on Radiological Protection publication 89 (*19*) adult human male and female models.

Because of the acquisition of dynamic images involved only the heart during the first 5 min, the brain, muscle, and urinary bladder were outside the field of view. The small bowel was sampled such that the volume of interest was within the field of view. Time–activity curves were linearly interpolated from time of injection to the first measurement with the organ in the field of view.

Minimal urinary excretion was observed, with low activity collecting in the urinary bladder, consistent with the previous rodent data (*16*). Thus, no excretion was modeled. Only physical decay was assumed after the last measurement. The body remainder was determined by subtracting all source organs from the calculated maximum integrated time–activity curve value of ^{11}C calculated from the reciprocal of the decay constant.

Dedicated Brain PET/CT and MR Image Acquisition and Processing

One additional participant underwent dedicated head and neck imaging using a Biograph Vision PET/CT scanner (Siemens). Low-dose CT was performed from the vertex to the cervicothoracic junction for anatomic alignment and attenuation correction. After injection of ^{11}C-CS1P1 and a saline flush, dynamic images were obtained from the vertex to about C5 for 2 h. The participant took a 15-min break after 60 min. PET images were reconstructed using a 3D ordered-subset expectation maximization algorithm with time-of-flight and point-spread-function resolution modeling (8 iterations and 5 subsets). For the purposes of this analysis, frames from 30 to 60 min were summed to create summed activity images and converted to an SUV image using the participant's measured body weight for normalization.

This participant also underwent 3-T head and neck MR scanning (Siemens Biograph mMR) using a 32-channel head and neck coil. A T1-weighted magnetization-prepared rapid-acquisition gradient-echo and T2-weighted 3D fluid-attenuation inversion recovery image was

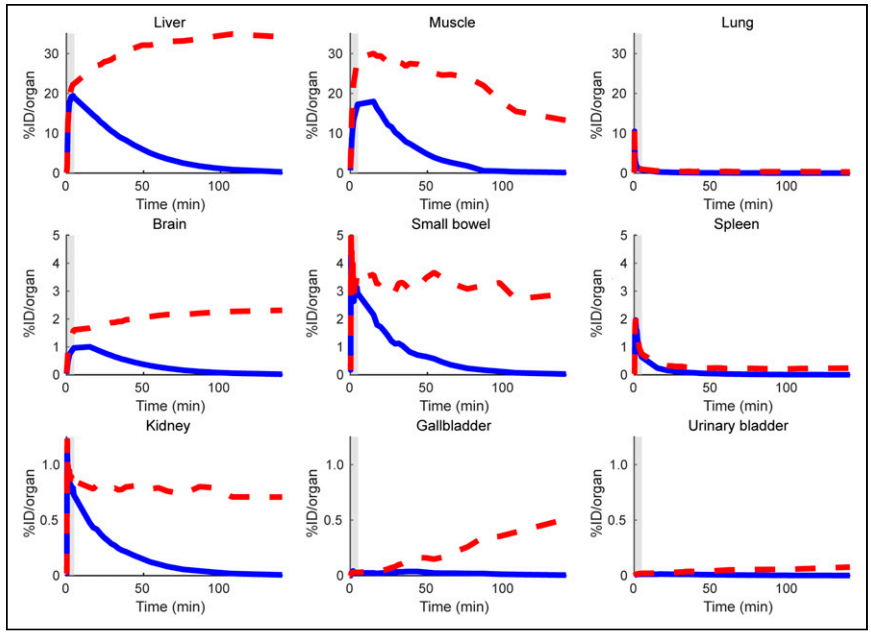

FIGURE 4. Non–decay-corrected (blue) and decay-corrected (red) time–activity curves for organs showing measurable signal. Axes vary in scale by row. Shaded area indicates first 5 min of scan, when dynamic images over heart were acquired. %ID = percentage injected dose.

TABLE 2
Integrated Time–Activity Curve Values (Minutes)

Site	Participant no. 1	2	3	4	5	6	7	8	9	10	Average	SD
Liver	6.45	5.15	6.85	6.75	6.16	7.41	7.36	4.24	7.76	5.55	6.37	1.11
Brain	0.45	0.39	0.61	0.40	0.38	0.43	0.49	0.29	0.27	0.43	0.41	0.10
Kidney	1.01	0.79	1.22	0.90	0.78	1.15	0.99	0.52	1.09	0.71	0.92	0.22
Small bowel	0.73	0.66	0.83	1.00	0.88	0.77	0.98	0.35	0.74	0.94	0.79	0.19
Lung	0.29	0.24	0.24	0.23	0.20	0.31	0.27	0.21	0.25	0.19	0.24	0.04
Left ventricular wall	0.16	0.85	0.19	0.28	0.27	0.31	0.31	0.12	0.28	0.18	0.30	0.21
Spleen	0.10	0.08	0.12	0.09	0.10	0.10	0.12	0.07	0.07	0.17	0.10	0.03
Gallbladder	0.01	0.02	0.02	0.01	0.01	0.02	0.03	0.01	0.03	0.02	0.02	0.01
Urinary bladder	0.01	0.00	0.02	0.01	0.02	0.06	0.01	0.01	0.01	0.01	0.01	0.02
Remainder	16.82	19.06	16.23	17.68	18.45	16.85	15.51	22.27	16.99	19.65	17.95	1.98

TABLE 3
Radiation Dosimetry, Female

Site	Participant no. 2	3	8	9	10	Mean	SD
Adrenals	5.68	6.56	5.28	6.77	6.07	6.07	0.61
Brain	2.06	2.89	1.75	1.57	2.25	2.10	0.51
Breasts	2.44	2.16	2.62	2.29	2.44	2.39	0.17
Esophagus	3.79	3.47	3.46	3.77	3.52	3.60	0.16
Eyes	2.20	1.98	2.50	1.95	2.28	2.18	0.23
Gallbladder wall	5.88	6.54	5.01	7.28	5.92	6.13	0.84
Left colon	3.47	3.07	3.55	3.21	3.40	3.34	0.20
Small intestine	3.26	3.13	3.46	3.25	3.43	3.31	0.14
Stomach wall	3.50	3.31	3.61	3.48	3.56	3.49	0.11
Right colon	12.40	14.70	8.35	13.50	16.40	13.07	3.03
Rectum	2.82	2.47	3.25	2.57	2.92	2.81	0.31
Heart wall	16.00	5.03	3.93	6.70	4.94	7.32	4.95
Kidneys	14.70	21.90	10.40	20.00	13.70	16.14	4.72
Liver	20.30	26.60	16.90	30.00	21.80	23.12	5.19
Lungs	3.12	3.00	2.73	3.22	2.78	2.97	0.21
Ovaries	2.97	2.64	3.36	2.74	3.08	2.96	0.29
Pancreas	4.75	5.04	4.68	5.39	4.95	4.96	0.28
Salivary glands	2.35	2.09	2.66	2.09	2.42	2.32	0.24
Red marrow	2.62	2.42	2.81	2.54	2.67	2.61	0.15
Osteogenic cells	2.26	2.06	2.48	2.13	2.31	2.25	0.16
Spleen	4.68	6.08	4.08	4.43	7.68	5.39	1.49
Thymus	3.25	2.63	3.13	2.83	2.94	2.96	0.24
Thyroid	2.52	2.18	2.77	2.29	2.52	2.46	0.23
Urinary bladder wall	2.39	2.26	2.86	2.19	2.52	2.44	0.26
Uterus	2.89	2.56	3.30	2.66	3.00	2.88	0.29
Total body	3.30	3.22	3.39	3.37	3.38	3.33	0.07
Effective dose (*18*)	4.13	4.32	3.69	4.49	4.28	4.18	0.30

Data are single-participant individual organ doses (μSv/MBq).

acquired for image registration and segmentation. This image was processed through FreeSurfer, version 7.2 (*20*), which identifies brain structures in a semiautomated manner. FreeSurfer segmentation and the summed activity images were aligned through affine registration (in-house software, https://4dfp.readthedocs.io) and the SUVs extracted from labeled regions. RNA expression, defined by microarray and expressed as *z* scores, were downloaded from the Allen Brain Atlas (2010) for S1PR1–5. Regions defined in both FreeSurfer and the Allen Brain Atlas and measurable without explicit partial-volume correction were extracted.

Statistical Analysis

Mean and SD for all measurements across individuals are provided. Male and female subjects are reported separately. We also compared the relationship between RNA expression (expressed as *z* scores from the Allen Brain Atlas) and ^{11}C-CS1P1 activity using a Pearson *r* test.

RESULTS

Participant Characteristics and Injected Dose

Table 1 provides demographic and radiopharmaceutical dosing information for the 10 dosimetry participants. The mean and SD of the administered mass of ^{11}C-CS1P1 was 3.15 ± 0.98 μg (range, 0.98–4.70 μg). The mean administered activity was 226.4 ± 71.97 MBq (range, 99.9–362.6 MBq).

Safety Events

There were no adverse or clinically detectable pharmacologic effects in any of the participants. No participants reported adverse reactions immediately after the scan. One participant reported mild flulike symptoms at the follow-up call. No participants reported headache, injection site reactions, or symptoms consistent with bradycardia.

No events of asymptomatic or symptomatic bradycardia, hypotension (systolic blood pressure < 100, diastolic blood pressure < 70), arrhythmias, or changes in complete blood count, comprehensive metabolic panel, or urinalysis were observed. Heart rate before injection, 5 min after injection, and at discharge, as captured on a 12-lead electrocardiogram, was stable in all participants (Fig. 1).

Qualitative Biodistribution (Dosimetry Cohort)

Male and female decay-corrected, summed activity images demonstrated significant uptake by the liver and, to a much lesser

TABLE 4
Radiation Dosimetry, Male

	Participant no.						
Site	1	4	5	6	7	Mean	SD
Adrenals	5.71	5.80	5.47	6.28	5.97	5.85	0.30
Brain	1.99	1.80	1.77	1.90	2.09	1.91	0.13
Esophagus	2.69	2.85	2.82	2.90	2.76	2.80	0.08
Eyes	1.62	1.69	1.75	1.62	1.52	1.64	0.09
Gallbladder wall	6.64	7.21	6.50	7.60	7.89	7.17	0.60
Left colon	2.60	2.73	2.75	2.70	2.54	2.66	0.09
Small Intestine	2.70	2.89	2.89	2.80	2.68	2.79	0.10
Stomach wall	2.81	2.95	2.94	2.99	2.84	2.91	0.08
Right colon	13.70	17.80	16.00	14.40	17.40	15.86	1.80
Rectum	2.11	2.22	2.30	2.15	1.98	2.15	0.12
Heart wall	4.07	5.61	5.47	6.14	6.03	5.46	0.83
Kidneys	16.30	14.90	13.10	18.40	16.10	15.76	1.95
Liver	19.90	20.90	19.10	22.80	22.60	21.06	1.63
Lungs	2.55	2.44	2.31	2.78	2.60	2.54	0.18
Pancreas	3.37	3.58	3.52	3.60	3.47	3.51	0.09
Prostate	2.14	2.26	2.33	2.20	2.02	2.19	0.12
Salivary glands	1.84	1.91	1.98	1.84	1.73	1.86	0.09
Red marrow	2.00	2.09	2.12	2.08	1.95	2.05	0.07
Osteogenic cells	1.87	1.95	1.99	1.91	1.79	1.90	0.08
Spleen	4.47	4.17	4.26	4.36	5.00	4.45	0.33
Testes	1.72	1.81	1.89	1.73	1.59	1.75	0.11
Thymus	2.20	2.36	2.39	2.36	2.22	2.31	0.09
Thyroid	1.95	2.03	2.09	1.99	1.84	1.98	0.09
Urinary bladder wall	2.02	2.12	2.36	2.59	1.92	2.20	0.27
Total body	2.39	2.51	2.52	2.50	2.37	2.46	0.07
Effective dose (*18*)	3.34	3.63	3.44	3.64	3.65	3.54	0.14

Data are single-participant individual organ doses (μSv/MBq).

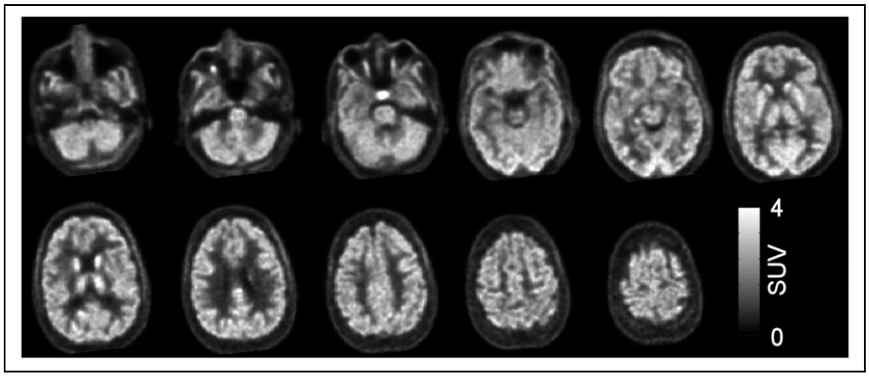

FIGURE 5. Summed brain activity images from 20 to 60 min after injection in single participant. Units are SUV based on measured body weight.

extent, kidneys (Fig. 2A). High activity was seen in the liver at early time points and in the gallbladder at later points (Fig. 2B). Activity accumulated in the small bowel at late time points, but since significant decay has occurred by 120 min (~6 half-lives) after injection, the radiation dose to the small intestine was minimal. These observations are compatible with hepatobiliary clearance. Minimal activity was observed in the urinary bladder and in the excreted urine (average urinary activity, 2.67 MBq).

^{11}C-CS1P1 uptake was next examined in more detail throughout the body (Fig. 3). Brain uptake was higher in gray matter, including subcortical structures, than in white matter (Fig. 3A). Notably, spinal uptake was minimal. Increased uptake was observed in the submandibular salivary glands (Fig. 3B), left ventricle (Fig. 3C), and liver and common bile duct (Fig. 3D). Low levels of activity were seen in the kidneys and the urinary bladder. No enlarged lymph nodes were identified in the 10 dosimetry participants.

Integrated Time–Activity

Integrated time–activity was calculated in organs demonstrating measurable activity (Fig. 4; Table 2). The highest integrated time–activity value was seen in the liver (6.37 ± 1.11 min). The mean integrated time–activity value of muscle was 5.51 ± 0.98 min (21% of injected dose) and was assigned to the remainder of the body in the OLINDA model. Another notable organ was the kidney (0.92 ± 0.22 min), but there was a minimal measurable integrated time–activity value in the urinary bladder (0.01 ± 0.02 min). A large fraction of the integrated time–activity was not measured in a specific organ (specifically measured, 34%; unmeasured, 66%) and thus was distributed into the remainder of the body.

Dosimetry

Dosimetry tables for women (Table 3) and men (Table 4) show the dose distribution calculated using OLINDA. The dose-limiting organ was the liver, with a dose of 23.12 μSv/MBq in women and 21.06 μSv/MBq in men. The effective dose was 4.18 μSv/MBq in women and 3.54 μSv/MBq in men. Using a maximum delivery dose of 740 MBq (20 mCi), the effective dose for women would be 3.1 mSv (0.31 rem), with a liver dose of 17.1 mSv (1.7 rem); the effective dose for men would be 2.6 mSv (0.26 rem), with a liver dose of 15.6 mSv (1.56 rem).

Brain-Specific Activity Analysis

The summed decay-corrected activity measured from 30 to 60 min after injection in a single participant is shown in Figure 5. Gray matter, specifically subcortical gray matter, had higher activity than white matter. Within gray matter, the visual cortex had relatively high activity whereas the temporal pole and medial temporal lobe had low activity. On the basis of a single participant, we present preliminary evidence that ^{11}C-CS1P1 selectively accumulates in brain regions that express S1PR1. In a small set of regions of interest, we found a strong correlation ($r = 0.84$, $P = 0.016$) between ^{11}C-CS1P1 activity (expressed as a z score compared with whole brain activity) and S1PR1 RNA expression (expressed as a z score) obtained from the Allen Brain Atlas (Fig. 6). We assessed the specificity of ^{11}C-CS1P1 for S1PR1 by examining the correlation between ^{11}C-CS1P1 binding and RNA expression of S1PR2–5. We found much weaker correlations with off-target S1PRs than with S1PR1 (Fig. 7; $r = 0.85$ vs. $r < 0.57$). These results suggest that ^{11}C-CS1P1 is successfully engaging the target in a specific manner.

DISCUSSION

We report the safety and dosimetry of intravenous administration of ^{11}C-CS1P1 to healthy human volunteers. No safety events were observed after injection. Dosimetry analysis revealed effective doses within acceptable limits, including the critical organ (liver). These results support the safety of ^{11}C-CS1P1 for human investigation.

S1PR1-modulating drugs, such as fingolimod, are approved for the treatment of relapsing–remitting multiple sclerosis. These drugs are highly efficacious, but fingolimod was associated with

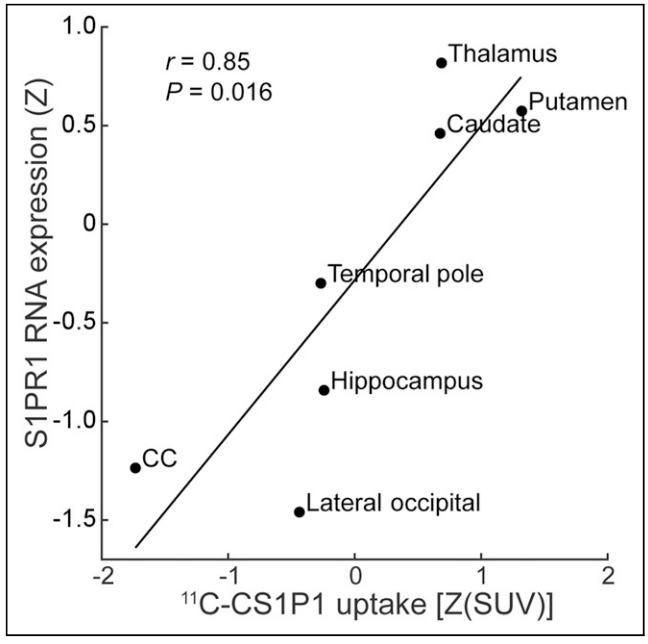

FIGURE 6. Correlation of ^{11}C-CS1P1 uptake with S1PR1 expression. Regional SUVs were extracted from summed activity image using FreeSurfer and then z-transformed. Matching S1PR1 RNA expression was extracted from Allen Brain Atlas and correlated. Tracer activity and RNA expression correlated significantly, thus providing preliminary evidence that ^{11}C-CS1P1 engages its target.

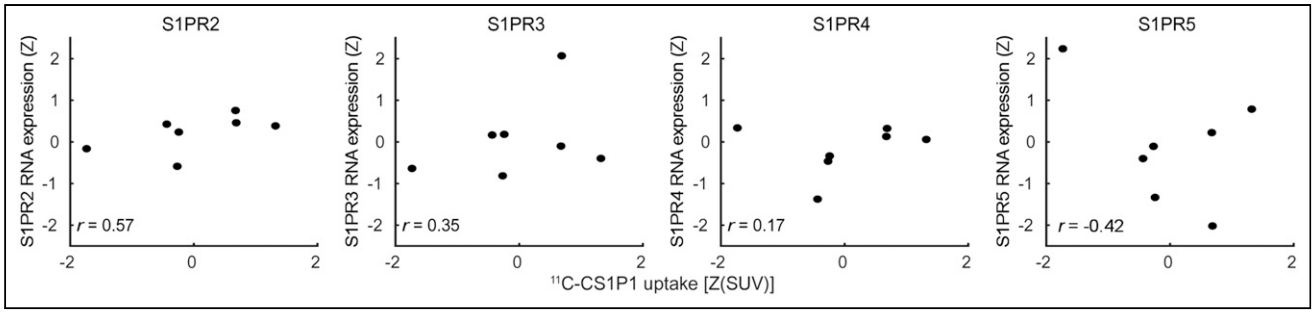

FIGURE 7. Lack of correlation between ^{11}C-CS1P1 uptake and S1PR2–5 expression. Scatterplots in same style as Figure 6 are shown. All correlations are smaller than correlation between ^{11}C-CS1P1 and S1PR1.

potentially significant bradycardia (*7*). The drug label requires cardiac monitoring for the first dose, and consequently, there was concern that ^{11}C-CS1P1 could similarly cause bradycardia despite the very low mass of CS1P1 injected. This safety study collected frequent electrocardiograms and performed telemetry monitoring and found no significant bradycardia or conduction abnormalities. Such abnormalities were not expected because of the low mass of ^{11}C-CS1P1 injected (3.15 ± 0.98 μg, compared with a fingolimod dose of 0.5 mg). In fact, heart rate tended to increase over the study, strongly suggesting a negligible effect of ^{11}C-CS1P1 on cardiac conduction. Finally, no significant laboratory abnormalities were identified. Thus, we conclude that, given the present exclusion criteria, ^{11}C-CS1P1 is a safe and well-tolerated radiotracer.

The critical organ was the liver, consistent with rodent dosimetry studies (*16*). The liver integrated time–activity curve value was 6.37 min and 8.34 min in the human and mouse, respectively. The calculated effective dose based on human measurement was 4.18 μSv/MBq in women and 3.54 μSv/MBq in men. For an injected dose of 740 MBq (20 mCi), the whole-body effective dose would be 3.1 mSv (0.31 rem) for women and 2.6 mSv (0.26 rem) for men. The liver effective dose would be 17.1 mSv (1.71 rem) for women and 15.6 mSv (1.56 rem) for men. As a comparison, the effective dose of ^{11}C-Pittsburgh compound B, a well-known marker of amyloid-β deposition in the brain associated with Alzheimer disease, is 4.74 μSv/MBq (*21*). This effective dose supports the safety and utility of ^{11}C-CS1P1 for human imaging from a radiation dose perspective.

The first 5 min of PET data were collected over the thorax to capture initial blood radioactivity and facilitate safety procedures. Thus, counts from some organs (e.g., brain) were not collected and were imputed for the early time points. This imputation was performed by linear interpolation from the injection time to the earliest measured time point. Other interpolation strategies were possible; however, such choices are arbitrary and would not meaningfully influence the calculated dosimetry. For example, the brain is the organ outside the initial field of view with the highest uptake but represents only about 1.5% of the total activity in the interval after the first 5 min. Thus, the choice to image initially over the thorax did not significantly impact the dosimetry calculation.

Review of CT images revealed no incidental abnormalities associated with increased ^{11}C-CS1P1 binding. However, the whole-body PET images inform the biology of the tracer. ^{11}C-CS1P1 is clearly metabolized by the liver. This conclusion is supported by the high liver activity, the late activity identified in the gallbladder, and the clear identification of the common bile duct on the basis of radioactivity. Renal uptake is likely not related to clearance since the collecting systems have little activity and only a small amount of activity was collected in the urinary bladder. Significant activity was also seen within the cardiac muscle, and S1P-based signaling is known to contribute to dose-related bradycardia in fingolimod (*7*). Salivary gland activity may be related to the role of S1P signaling in salivary gland diseases such as Sjogren syndrome (*22*).

Finally, we present preliminary evidence in a single participant that ^{11}C-CS1P1 selectively accumulates in brain regions that have greater S1PR1 expression. Ongoing work in a larger cohort will determine whether this finding can be confirmed. We note that this finding is compatible with animal work that demonstrates similar tracer behavior in animals (*4*).

CONCLUSION

We present human safety and dosimetry data supporting the application of ^{11}C-CS1P1 to the study of human disease. This radioligand is well tolerated from both a medical and a radiologic perspective. Future studies will explore the utility of this tracer for the study of multiple sclerosis and other inflammatory diseases.

DISCLOSURE

This work was supported by the U.S. National Institutes of Health (NIH) (R01NS103988, R01AG054567, P01AG003991, and U19 AG032438) and by the National Institute of Neurological Disorders and Stroke, National Institute on Aging (NS103988, NS107281, and NS075527). Matthew R. Brier was supported by 2R25NS090978-06. Dean F. Wong was supported by the National Institute of Mental Health (7R01MH10719705). Joel S. Perlmutter was supported by the Barnes Jewish Hospital Foundation (Stein Family Fund), Riney Foundation, N. William Grant Fund, American Parkinson Disease Association (APDA), and Greater St. Louis Chapter of the APDA. No other potential conflict of interest relevant to this article was reported.

KEY POINTS

QUESTION: Is ^{11}C-CS1P1 safe for use in human imaging?

PERTINENT FINDINGS: ^{11}C-CS1P1 was not associated with any adverse effect. Dosimetry is compatible with longitudinal human imaging.

IMPLICATIONS FOR PATIENT CARE: ^{11}C-CS1P1 is safe for human use and can be used to study inflammation in diseases such as multiple sclerosis.

REFERENCES

1. Proia RL, Hla T. Emerging biology of sphingosine-1-phosphate: its role in pathogenesis and therapy. *J Clin Invest.* 2015;125:1379–1387.
2. Peyrin-Biroulet L, Christopher R, Behan D, Lassen C. Modulation of sphingosine-1-phosphate in inflammatory bowel disease. *Autoimmun Rev.* 2017;16:495–503.
3. Lee MJ, van Brocklyn JR, Thangada S, et al. Sphingosine-1-phosphate as a ligand for the G protein-coupled receptor EDG-1. *Science.* 1998;279:1552–1555.
4. Liu H, Jin H, Yue X, et al. PET imaging study of S1PR1 expression in a rat model of multiple sclerosis. *Mol Imaging Biol.* 2016;18:724–732.
5. Jackson SJ, Giovannoni G, Baker D. Fingolimod modulates microglial activation to augment markers of remyelination. *J Neuroinflammation.* 2011;8:76.
6. Maceyka M, Spiegel S. Sphingolipid metabolites in inflammatory disease. *Nature.* 2014;510:58–67.
7. Kappos L, Antel J, Comi G, et al. Oral fingolimod (FTY720) for relapsing multiple sclerosis. *N Engl J Med.* 2006;355:1124–1140.
8. Brinkmann V. FTY720 (fingolimod) in multiple sclerosis: therapeutic effects in the immune and the central nervous system. *Br J Pharmacol.* 2009;158:1173–1182.
9. Miron VE, Ludwin SK, Darlington PJ, et al. Fingolimod (FTY720) enhances remyelination following demyelination of organotypic cerebellar slices. *Am J Pathol.* 2010;176:2682–2694.
10. Choi JW, Gardell SE, Herr DR, et al. FTY720 (fingolimod) efficacy in an animal model of multiple sclerosis requires astrocyte sphingosine 1-phosphate receptor 1 (S1P1) modulation. *Proc Natl Acad Sci USA.* 2011;108:751–756.
11. Watson C, Long JS, Orange C, et al. High expression of sphingosine 1-phosphate receptors, S1P1and S1P3, sphingosine kinase 1, and extracellular signal-regulated kinase-1/2 is associated with development of tamoxifen resistance in estrogen receptor-positive breast cancer patients. *Am J Pathol.* 2010;177:2205–2215.
12. LaMontagne K, Littiewood-Evans A, Schnell C, et al. Antagonism of sphingosine-1-phosphate receptors by FTY720 inhibits angiogenesis and tumor vascularization. *Cancer Res.* 2006;66:221–231.
13. Sukocheva O, Wadham C, Gamble J, Xia P. Sphingosine-1-phosphate receptor 1 transmits estrogens' effects in endothelial cells. *Steroids.* 2015;104:237–245.
14. Liu H, Jin H, Yue X, et al. PET study of sphingosine-1-phosphate receptor 1 expression in response to vascular inflammation in a rat model of carotid injury. *Mol Imaging.* 2017;16:1536012116689770.
15. Liu H, Jin H, Han J, et al. Upregulated sphingosine 1-phosphate receptor 1 expression in human and murine atherosclerotic plaques. *Mol Imaging Biol.* 2018;20:448–456.
16. Liu H, Laforest R, Gu J, et al. Acute rodent tolerability, toxicity, and radiation dosimetry estimates of the S1P1-specific radioligand [^{11}C]CS1P1. *Mol Imaging Biol.* 2020;22:285–292.
17. Luo Z, Gu J, Dennett RC, et al. Automated production of a sphingosine-1 phosphate receptor 1 (S1P1) PET radiopharmaceutical [^{11}C]CS1P1 for human use. *Appl Radiat Isot.* 2019;152:30–36.
18. The 2007 recommendations of the International Commission on Radiological Protection. ICRP publication 103. *Ann ICRP.* 2007;37:1–332.
19. Basic anatomical and physiological data for use in radiological protection: reference values. A report of age- and gender-related differences in the anatomical and physiological characteristics of reference individuals. ICRP Publication 89. *Ann ICRP.* 2002;32:5–265.
20. Fischl B. FreeSurfer. *Neuroimage.* 2012;62:774–781.
21. Scheinin NM, Tolvanen TK, Wilson IA, Arponen EM, Någren KÅ, Rinne JO. Biodistribution and radiation dosimetry of the amyloid imaging agent ^{11}C-PIB in humans. *J Nucl Med.* 2007;48:128–133.
22. Seo J, Koo NY, Choi WY, et al. Sphingosine-1-phosphate signaling in human submandibular cells. *J Dent Res.* 2010;89:1148–1153.